Investigation of the Kelvin-Helmholtz Instability Process in Liquefying Hybrid Rocket Fuels

SEVILLE, SPAIN / 14 – 18 MAY 2018

Anna Petrarolo [(1)], Mario Kobald [(2)], Stefan Schlechtriem [(3)]

German Aerospace Center (DLR)
Institute of Space Propulsion
Lampoldshausen, 74239 Hardthausen, Germany

[(1)] PhD Candidate, Propellants Department, DLR Lampoldshausen, anna.petrarolo@dlr.de
[(2)] Group Leader, Propellants Department, DLR Lampoldshausen, mario.kobald@dlr.de
[(3)] Director, DLR Lampoldshausen

KEYWORDS: Hybrid rocket propulsion, Paraffin fuel, Optical Investigation, Proper Orthogonal Decomposition, Independent Component Analysis, Kelvin-Helmholtz instability.

ABSTRACT:

The combustion behaviour of paraffin-based hybrid rocket fuels has been investigated with different optical techniques in the framework of this research. Combustion tests were conducted in a 2D single-slab burner at atmospheric conditions. High speed videos and CH* chemiluminescence imaging were performed and analysed in detail by using an automated video evaluation routine. Two different decomposition techniques (Proper Orthogonal Decomposition and Independent Component Analysis) were applied to the scalar field of the flame luminosity and the flame characteristics of these fast burning fuels were computed. The fuel viscosity and oxidizer mass flow have been varied in order to study the influence of these parameters on the liquid layer instability process. Wave-like structures can be seen throughout the whole combustion process in all the performed tests. The flame topology and location within the boundary layer is found to depend on the choice of the fuel and oxidizer mass flow.

1. INTRODUCTION

1.1 Hybrid Rocket Engines

Hybrid rocket engines (HRE) typically consist of a solid fuel and a liquid or gaseous oxidizer. Due to the fact that the propellants are stored in two different states of matter, HRE have some advantages compared to classical solid or liquid rocket engines. Considering storage and handling, they are safer than solid motors and more tolerant to cracks. This also contributes to reduce the total cost of the engine. Moreover, they are characterized by controllable thrust, including shut off and restart capability. With respect to liquid engines, they are easier to throttle, mechanically less complex and, consequently, cheaper [1]. However, HRE are historically characterized by low combustion efficiency, due to the typical diffusive flame, and low regression rate, due to the use of polymeric fuels, such as Hydroxyl-terminated Polybutadiene (HTPB) or High-Density Polyethylene (HDPE). In fact, the regression rate of classical polymeric hybrid fuels is diffusion limited and hindered by the blocking effect. In a HRE the combustion occurs in the turbulent boundary layer over the fuel surface and the flame is located where there is a combustible ratio between the vaporized oxidizer and fuel [2]. The heat is then radiated and convected from the diffusion flame to the fuel surface. In a classical hybrid, the polymeric fuel pyrolyses and its vapors are transported to the diffusion flame where it reacts with the atomized oxidizer transported from the free stream via turbulent diffusion [3]. The problem of the low performance of HRE was overcome in the past by increasing the fuel burning area with the use of multi-port fuel grains, which, on the other hand, increase the complexity of the system and the residual mass of unburned fuel (which leads to a decrease in the delivered specific impulse).

The discovery of a new class of high regression rate hybrid rocket fuels at Stanford University has renewed the interest in hybrid rockets. These fast-burning fuels are characterized by low viscosity and surface tension [4], thus allowing for a different combustion mechanism. The so-called liquefying fuels form a thin liquid layer on the fuel surface during the combustion [5], which becomes unstable under the oxidizer flow. It is expected that the shear forces between the liquid layer and the

oxidizer flow are able to trigger the Kelvin-Helmholtz instability process: roll waves are produced in the liquid layer and fuel droplets are forced to separate and entrain into the flow [6], see also Fig.1. The entrainment mechanism works like a spray injection along the length of the motor, which increases the effective fuel burning area and reduces the blocking effect and the effective heat of gasification. This enables simple, single-port fuel grain designs and makes hybrid propulsion a competitive candidate for launch systems and in-space missions.

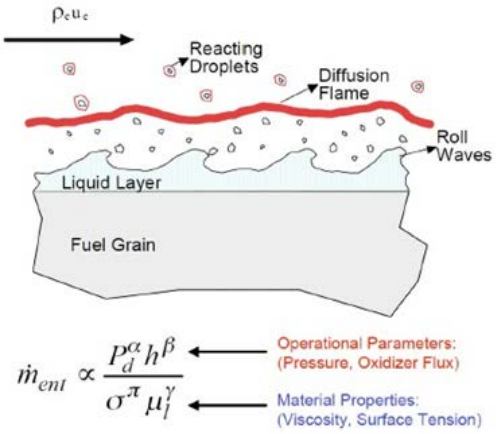

Figure 1: Liquefying fuel combustion theory, taken from [12],[13]

A visualization of the entrainment process with paraffin-based fuels, obtained within this research, is shown in Fig.2. Since 2013, many optical investigations on liquefying hybrid rocket fuels have been done at the German Aerospace Center (DLR), to better understand the entrainment process. Latest works investigate in detail the liquid layer instability process and the combustion parameters that trigger and influence it [7], [8], [9]. Recent tests with different paraffin-based fuels and gaseous oxygen (GOX) showed an exponential relation between the liquid layer viscosity and the overall regression rate [10], which proves the predicted entrainment correlation in Fig.1.

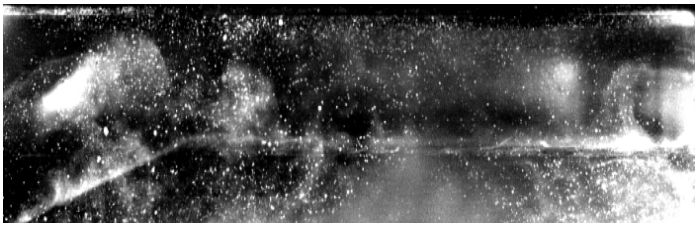

Figure 2: Liquefying fuel combustion image created within this research (oxidizer mass flow from left to right)

1.2 Optical Investigations of Hybrid Rocket Combustion

The discovery of liquefying hybrid rocket fuels has revitalized researches in hybrid propulsion and, in particular, in optical investigations of the hybrid rocket combustion process, in order to capture the entrainment. To fully understand this phenomenon, it is necessary to adapt the liquid layer stability theory, extensively studied in the past [11], [12], to the typical operating conditions that are encountered in hybrid combustion. This means that the behavior of films has to be studied under strong blowing conditions and relatively high liquid Reynolds numbers. The Kelvin-Helmholtz instability (KHI) theory and the liquid layer break up process, which leads to the fuel droplet entrainment, have been well examined in the literature [5], [6], [13], [14], [15]. At high Reynolds numbers, a roll wave mechanism for the liquid entrainment is suggested [15]. One of the most important experimental works on the entrainment is done by Gater and l'Ecuyer [16]. They performed tests in a wind tunnel, in order to study the entrainment rates of thin films of different liquids under strong gas flow conditions. Some tests were performed with hot gas flow. On the basis of these experiments and their results, Karabeyoglu et al. [5], [6] suggested the droplet entrainment mechanism in hybrid rocket engines. However, the dependence of the entrainment mass transfer on the experimental parameters is different in every study and needs to be assessed on a case-by-case basis. Consequently, many optical investigations on the hybrid combustion process have been performed in recent years.

In 2011, Nakagawa et al. investigated the dependence of the regression rate on the fuel viscosity. They performed optical tests at atmospheric pressure with different paraffin-based fuels and gaseous oxygen. Their images showed that droplets are generated during the combustion and entrained in the flow [17].

Many optical investigations on the combustion behavior of both polymeric and paraffin-based hybrid rocket fuels have been done at the Stanford Combustion Visualization facility. In 2012, Chandler et al. investigated the combustion of paraffin-based fuels with gaseous oxygen at both atmospheric and elevated pressures. Their results showed roll waves and droplets in the atmospheric tests and filament-like structures along the sides of the fuel grains in the tests run at elevated pressures [18]. In 2014-2016, many optical tests were conducted from Jens et al. with the same facility. They performed Schlieren and OH* images of the combustion of different classical polymeric and paraffin-based fuels in combination with gaseous oxygen at both atmospheric and elevated pressures [19]. They reported unsteady blowing

events of paraffin droplets in the tests at higher pressure, slightly above the critical pressure of their paraffin samples. Schlieren results of their tests reported a thickening boundary layer with increasing pressure [20].
In 2014, Wada et al. visualized the combustion of different polymeric and paraffin fuels at a pressure ranging from 1 up to 20 bar. In contrast to the other mentioned optical experiments, this set-up looks at the combustion of opposing slabs of fuel mounted vertically. From their observations, they concluded that both the number and size of the entrained droplets are independent of the chamber pressure [21].
Since 2013, many optical investigations have been conducted at the German Aerospace Center (DLR), Institute of Space Propulsion in Lampoldshausen. Kobald et al. performed visual and Schlieren images of the combustion of paraffin wax and gaseous oxygen at atmospheric pressure. They reported visualization of droplets entrainment during start-up and shut-down transients [22], [23]. Since 2015, an automated video evaluation routine has been developed in DLR, in order to capture the dominant flow dynamic and combustion behavior of paraffin-based hybrid rocket fuels during a typical test [24], [25], [26]. The latest results of this research are presented in this paper.

2. EXPERIMENTAL SET-UP

2.1 Paraffin-based fuels

Three different paraffin-based fuels have been investigated in the framework of this research. The wax that has been used as a baseline for all the fuels is type 6805 from the manufacturer Sasol Wax. It has been chosen because of its viscosity and surface tension values, which are the two fuel parameters that are expected to have the biggest influence on the entrainment process (see also Fig.1). Detailed laboratory experiments have been performed before, in order to measure these two parameters for the different fuels (see Petrarolo et al. [26]). All samples for the ballistic tests have been blackened by additives during fabrication to limit radiation effects during combustion to the fuel surface. Generally, the amount of blackening additive was less than 2% and has therefore negligible impact on the performance [27]. Three different percentages of a commonly available polymer have also been added to the paraffin samples, in order to have different viscosity values. In this way it was possible to study the influence of this parameter on the entrainment process. Moreover, the addition of polymer increases the mechanical properties of the paraffin, thus increasing also the quality of the combustion visualizations (less polluted window). All the investigated fuel slabs have been manufactured with a 20° forward facing ramp angle (see Fig.3), due to the better flame holding and, consequently, higher flame quality.

Figure 3: Fuel slab used in this research, before (top) and after (bottom) combustion test

2.2 Test Set Up and Data Acquisition

The experimental tests were performed at the Institute of Space Propulsion at the DLR Lampoldshausen, test complex M11. An already existing modular combustion chamber, used in the past to investigate the combustion behavior of solid fuel ramjets, was adjusted and used for the test campaigns [28]. A side view of the whole combustion chamber set-up is shown in Fig. 4. The oxidizer main flow is entering the combustion chamber from the left, after having passed two flow straighteners. The mass flow rate is adjusted by a flow control valve and it is measured with a Coriolis flow meter. A high frequency static pressure sensor is mounted in the combustion chamber. Ignition is done via an oxygen/hydrogen torch igniter from the bottom of the chamber. A test sequence is programmed before the test and is run automatically by the test bench control system. More details about the test bench and test settings are given in Kobald et al. and Petrarolo et al. [29], [24], [25].

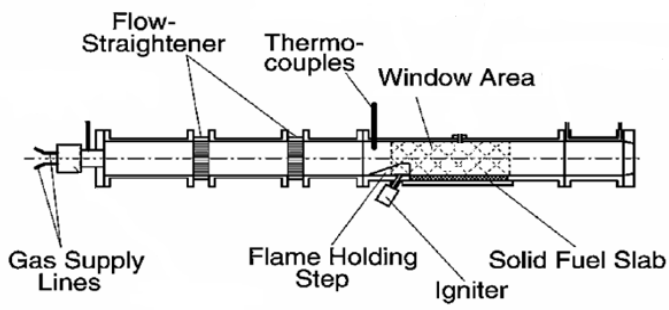

Figure 4: Side view of the combustion chamber set-up

In the framework of this research, all tests were done at atmospheric pressure and with an oxidizer mass flow ranging from 10 to 120 g/s. Combustion tests were performed using a single-slab paraffin-based fuel in combination with gaseous oxygen.

Three fuel slab configurations with different forward facing ramp angle were tested. All fuel slabs, produced and machined according to the same procedure, were 200 mm long, 100 mm wide and 20 mm high. Burning time was 3 seconds for each test. For video data acquisition a Photron Fastcam SA 1.1 high speed video camera was used with a maximum resolution of 1024x1024 pixel. The frame rate, resolution and shutter time of the camera were adjusted for each test, according to the test conditions and position of the camera. For the CH* chemiluminescence imaging a band-pass filter centered around 431 nm was placed in front of the camera. The excited CH* molecules emit photons around this wavelength, when they relax back to a lower energy state. Since high CH* concentration exists only in the main reaction zone, the resulting images provide a good indication of the instantaneous flame sheet location and topology.

3. METHODOLOGY FOR THE VIDEO ANALYSIS

3.1 High speed videos

The combustion high-speed videos are analyzed with a Matlab® routine, which returns as results the most excited frequencies and wavelengths characterizing the liquid melt layer. The video analysis is divided into three main phases:

- *video pre-processing*, where the video is modified and the Snapshot Matrix is created;
- *decomposition* of the Snapshot Matrix red into the spatial and temporal coefficients matrices with the two methods: Proper Orthogonal Decomposition (POD) and Independent Component Analysis (ICA);
- *post-processing*, where the Power Spectral Density (PSD) of spatial and temporal coefficients is performed.

As first step, a video pre-processing is performed, see Fig.5. During this phase, the images are exported from the video and cropped with the Software VirtualDub. Usually filters are added, to adjust the brightness and the contrast of the images. The function sharpen is also used to enhance the contrast of adjacent elements. There exists also lateral burning at the sides of the fuel, so the bottom of the fuel is cropped just up to the solid fuel surface, to reduce noise and errors. Yet, the size of the area of interest is kept as large as possible in order to capture the flow dynamics on the whole upper surface of the fuel slab. The angled front and the rear end, where further vortices are created, are not included in the frames. It is important to underline that the analyzed window has the same size in all the videos (500x60 pixel) and it is able to catch all the phenomena we are interested in, still leaving out sources of noise and errors (such as the aft and rear end of the slab and the bottom of the fuel). The images are then exported to Matlab® and converted from true-color RGB to binary data images, based on a luminance threshold. The background noise, which usually consists of small light spots (most likely burning paraffin droplets), is removed. Finally, the waves edge is automatically detected and a sparse matrix is created. Each frame is then rearranged as a column vector and the Snapshot Matrix, which contains all the frames to analyze, is created. It has to be noticed that the recorded video data is a line of sight measurement. Thus, the data in the analysis represent an integrated measurement over the whole fuel slab width.

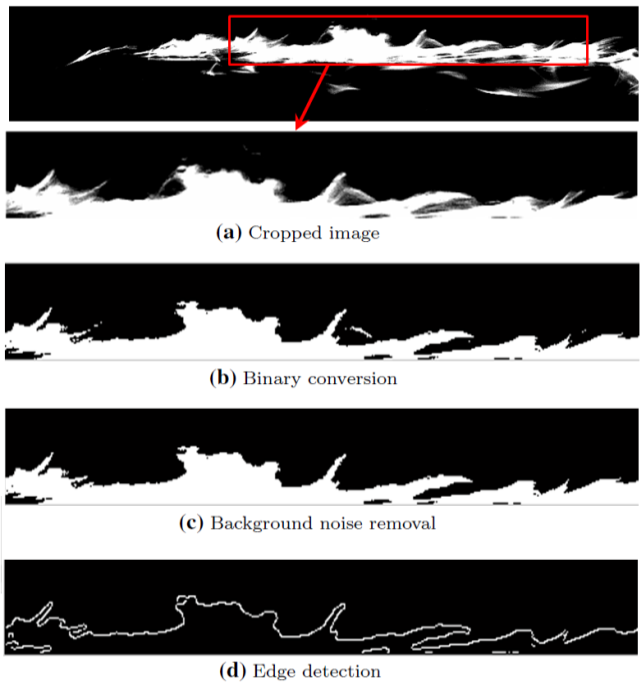

Figure 5: Video pre-processing steps

In a second step, the Snapshot Matrix is decomposed with both techniques, POD and ICA, into two matrices containing spatial and temporal coefficients.
The POD is a statistical method where an orthogonal transformation is used to convert a set of data into a set of linearly uncorrelated variables, which are called principal components. This method identifies the most coherent and energetic structures of the data. This enables us to retain only the dominant modes and to filter out the presence of the measurement noise, thus providing a good characterization of the dynamics of the problem. POD is also able to explicitly separate the spatial and time information [30]. On the other hand, the linear nature of the method can be a restriction for some data sets.

The ICA is a statistical and computational technique for revealing hidden components that underlie the observed data. The transformed variables correspond to the underlying components that describe the essential structure of the data and that correspond to some physical causes involved in the process. The ICA is a much more powerful method with respect to the POD. The basic functions found by the POD are uncorrelated but not statistically independent. This means that higher order dependencies still exist and, therefore, they are not properly separated. In other words, all POD modes contain some elements of all structures found in all of the fields [31]. On the other hand, ICA is able to search for basic functions that are statistically independent or as independent as possible, increasing the independence to higher statistical orders. When deriving these components, the data are separated into either spatially (sICA) or temporally (tICA) independent components; each choice yields corresponding statistically independent images or time courses.

Both methods are applied to the analysis of the luminosity field of images (scalar field) in a reactive flow. With POD, the considered scalar field is decomposed into mean, coherent and incoherent parts via statistical methods. In general, the coherent part includes all fluctuations possessing a somehow structured feature over the burning process. The incoherent part includes all fluctuations for which no pattern can be identified over the burning process. It is commonly thought that the first few modes correspond to the average structure of the data, while higher order modes contain information about fluctuations [32]. For what concerns ICA, since the aim of the present work is to identify independent spatial structures evolving in time, the spatial ICA is applied to the analysis of the luminosity field of the combustion process in a hybrid engine. This allows the identification of the leading independent structures during the burning process.

At the end of both algorithms, the Power Spectral Density (PSD) of the temporal and spatial coefficients is performed, in order to obtain the most excited frequencies and wavelengths during the combustion. The PSD of the temporal coefficients reveals whether there are dominant harmonics in the signal. The PSD of the spatial coefficients reveals the dominant wavelengths describing the change in luminosity in the horizontal or vertical direction. The column-wise spectral content of the spatial coefficients is related to the wavelength of the longitudinal waves, which are mainly moving in the horizontal direction. The row-wise spectral content is related to the position of the main flame above the fuel slab. In this work, only the results about the position of the main flame are presented. Moreover, it is important to underline that all the tests were analyzed with both decomposition methods. A comparison of the results given by the two methods was necessary in order to better characterize the dynamic of the process. In fact, both methods yield a whole range of different frequencies and wavelengths, which are amplified during the combustion. Some of them are related to the main dynamics of the combustion process, others are just random appearing vortices or not so energetic periodic signal (such as noise). In order to understand which frequencies and wavelengths are actually related to the main combustion events, it was necessary to compare the results of the two methods. If a frequency peak appears only in the POD, this is most likely related to a random energetic vortex (POD recognizes the most energetic structures in the flow field). On the other hand, if a frequency peak appears only in the ICA, this is most likely a periodic but not energetic signal, so not important (ICA recognizes periodic independent structures). Those peaks which appear in both methods are periodic and energetic signals, so related to the main events during the combustion process. So, at the end, only those frequencies and wavelengths appearing in both methods were considered. Further details of the applied methods are given in Kobald et al. [24] and Petrarolo et al. [25].

3.2 CH* chemiluminescence videos

For the CH* videos investigation, the flame zone is analyzed with the decomposition algorithms. The same procedure as for the high-speed video imaging is applied. However, the pre and post-processing are a bit modified, since the focus is now not on the frequencies and wavelengths peaks anymore. In particular in the pre-processing, the same cropping window as in the high-speed video frames is used, but no binary conversion is performed. The RGB images are converted to greyscale ones, so that the information on the flame luminosity field is not lost. Consequently, no edge detection is applied. Each frame is then rearranged as a column vector and the Snapshot Matrix, which contains all the frames to analyze, is created. The data matrix is decomposed with both techniques, POD and ICA, into two matrices containing spatial and temporal coefficients, like already explained for the high-speed videos. In the post-processing, the PSD of the temporal and spatial coefficients is replaced by the contour plots of the spatial coefficients (of both POD modes and independent components), which represent on a color map the intensity of the flame luminosity. In this way, it is possible to detect, within the flame zone, those areas where the reactions are more concentrated, independently from time.

4. KELVIN-HELMHOLTZ INSTABILITY

The Kelvin-Helmholtz instability (KHI) is an instability that arises in parallel shear flows where a discontinuity in velocity is present. The entrainment mechanism is dominated by the KHI behavior. The onset of KHI, which depends on the Reynolds number based on the liquid properties, is a necessary condition for droplets entrainment. The unstable waves then break up into droplets by the Plateu-Rayleigh instability mechanism (primary break-up). Droplets entrainment occurs from the unstable waves when the interfacial shear force between the two fluids exceeds the retaining force of surface tension [15], [33]. Droplets are then accelerated by the main gas flow and break up into smaller droplets or rebound. This mechanism is also referred as secondary instability (see Fig. 6).

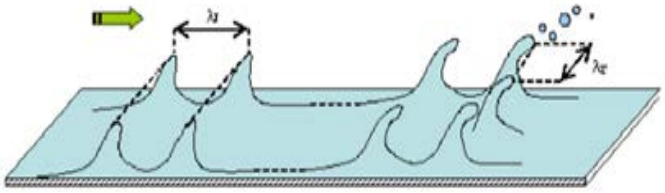

Figure 6: Kelvin-Helmholtz Instability, taken from [34].

In this work, the stability of a stratified gas-liquid flow is studied in a 2D domain for a horizontal channel configuration [14]. According to the Squire's Theorem, a two dimensional system is always more unstable than any equivalent three dimensional system. This means that KHI can be fully described and analyzed using a 2D domain. The model used in this analysis is shown in Fig.7. The coordinate y was neglected, so that a 2D bounded model could be studied.

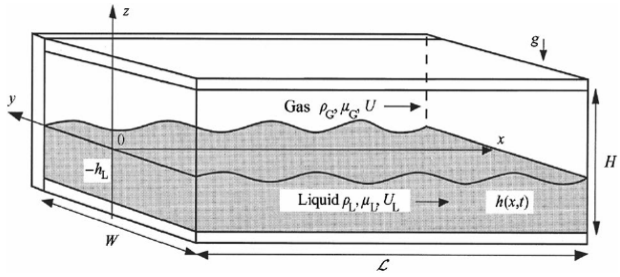

Figure 7: Kelvin-Helmholtz Instability bounded model, adapted from [14]

The governing equations used for describing the KHI problem are the Navier-Stokes and the continuity equations for viscous Newtonian fluids. The fuel liquid layer is considered at rest and the combustion products gas flow is moving at a fixed velocity. The only considered external force is the gravitational one. The effect of viscosity on shear stress is neglected and both fluids are considered homogeneous and irrotational. The equations are linearized and sinusoidal solutions are applied [14]. A small sinusoidal perturbation h is introduced at the interface between the gas and the liquid:

$$h(x,t) = Be^{ikx-i\omega t} \qquad (1)$$

Here the complex wave frequency ω gives information about the temporal stability, while the complex wave number k gives information about the spatial stability. For $\omega_I = 0$ neutral temporal stability is achieved, $\omega_I > 0$ indicates temporal instability, while $\omega_I < 0$ indicates temporal stability. In the same way, we get spatial instability for $k_I < 0$, stability for $k_I > 0$ and neutral stability for $k_I = 0$.
Solving the equations leads to the dispersion relation:

$$K_o\omega^2 + 2K_1\omega + K_2 = 0 \qquad (2)$$

where $K_0 = a_G\rho_G + a_L\rho_L$
$K_1 = -kUa_G\rho_G + ik^2(a_G\mu_G + a_L\mu_L)$
$K_2 = [U^2k^2a_G\rho_G - kg(\rho_L - \rho_G) - \gamma k^3]$

In order to find the neutral curve, we need to search for those values of the parameters for which the roots of the dispersion relation (2) are real (note that $\omega = \omega_R + i\omega_I$). By manipulating the dispersion relation and solving it with respect to the gas flow speed U, the neutral curve is obtained:

$$U^2 = g\frac{(a_L\mu_L + a_G\mu_G)^2}{a_La_G^2\mu_G^2 + \rho a_Ga_L^2\mu_L^2}\left(\beta^2k + \frac{1-\rho}{k}\right) \qquad (3)$$

where $a_L = \coth(kh_L)$; $a_G = \coth(kh_G)$; $\rho = \frac{\rho_G}{\rho_L}$; $\beta = \sqrt{\frac{\gamma}{g\rho_L}}$.

Figure 8 shows the neutral curves for pure paraffin 6805 at different mixture ratios OF (ratio between oxidizer and fuel mass flows). The values of liquid fuel density and viscosity are taken from the measurements done in the chemical laboratory. A liquid layer temperature of around 300°C is considered (averaged temperature between melting and boiling points). The gas density and viscosity values at each mixture ratio OF are given by the software NASA CEA (Chemical Equilibrium with Applications) at optimum conditions. The local minimum of each curve shows the critical wave number and corresponding critical gas velocity. The critical wavelength is the first unstable wave that is excited and it appears when the critical gas speed is reached. For gas speed below the critical one no instability is achieved. The critical values are influenced by the liquid viscosity (see Fig. 9).

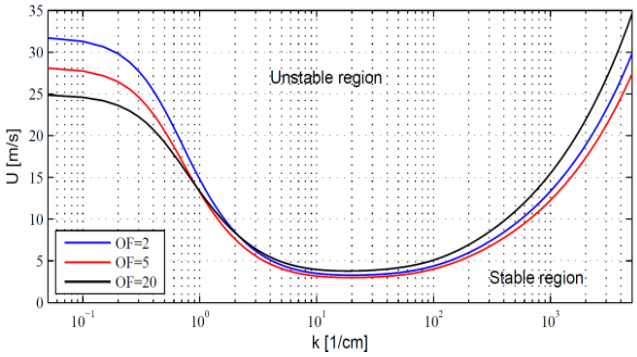

Figure 8: neutral curve of pure 6805. For each OF, the unstable region is for speeds above the corresponding curve; the stable region is below each curve.

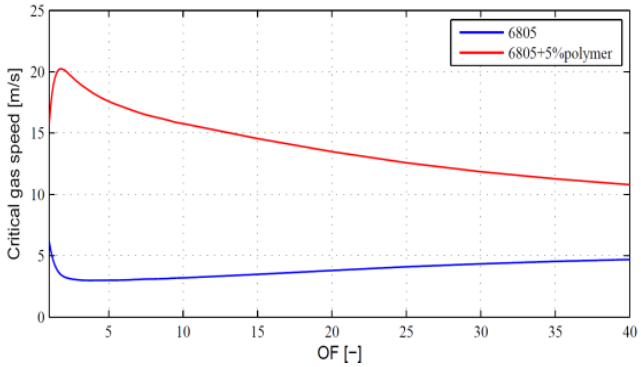

Figure 9: Influence of OF and fuel viscosity on the critical gas speed.

5. RESULTS AND DISCUSSION

In this paper, the influence of the oxidizer mass flow and fuel viscosity on the entrainment process is discussed. These are the two parameters that are expected to have the biggest influence on the droplets entrainment process, as shown in Fig.1 (the oxidizer mass flow is not explicitly included in the arguments of the equation in Fig.1, but it is influencing the entrainment mass flow through the dynamic pressure, with flow density and speed). Therefore, two main test campaigns were performed: pure paraffin 6805 and the same paraffin with 5% polymer were analysed with an oxidizer mass flow varying in a range from 10 to 120 g/s. In a previous test campaign [7], the influence of the forward facing ramp of the fuel slab was investigated with a fixed oxidizer mass flow and the main frequencies and wavelengths characterizing the entrainment process were identified. Therefore, in these test campaigns it was possible to study the influence of the fuel viscosity and oxidizer mass flow on the liquid layer break-up process, independently from the fuel configuration. Fuel slabs with 20° forward facing ramp were used, due to the better flame quality (i.e. better flame holding and continuous flame front).

5.1 High-speed videos

High speed videos of the combustion tests were recorded and analyzed, as explained in Sec. 3. By analyzing the PSD results of both POD and ICA, it is possible to obtain the most excited frequencies and wavelengths for each of them. As already written in Sec. 3, the PSD of the temporal coefficients reveals whether there are dominant harmonics in the signal. The PSD of the spatial coefficients reveals the dominant wavelengths describing the change in luminosity in the horizontal or vertical direction. The column-wise spectral content of the spatial coefficients is related to the wavelength of the longitudinal waves, which are mainly moving in the horizontal direction. The row-wise spectral content is related to the position of the main flame above the fuel slab. Moreover, it is important to underline that, in order to better characterize the dynamic of the process, a combination of the two decomposition techniques was necessary. In fact, both methods yield a whole range of different frequencies and wavelengths, which are amplified during the combustion. Some of them are related to the main dynamics of the combustion process, others are just random appearing vortices or not so energetic periodic signal (such as noise). In order to understand which frequencies and wavelengths are actually related to the main combustion events, it was necessary to compare the results of the two methods. If a frequency peak appears only in the POD, this is most likely related to a random energetic vortex (POD recognizes the most energetic structures in the flow field). On the other hand, if a frequency peak appears only in the ICA, this is most likely a periodic but not energetic signal, so not important (ICA recognizes periodic independent structures). Those peaks which appear in both methods are periodic and energetic signals, so related to the main events during the combustion process. So, at the end, only those frequency and wavelength peaks appearing in both methods were considered. The results about the frequencies and longitudinal wavelengths can be found in previous papers by Petrarolo et al. (see [7], [8], [9], [25], [26]). In this paper, the results about the position of the main flame over the fuel surface and the flame thickness are presented. As already done for the previous investigations, the analysis was carried out on 1 second (10000 frames) during the steady-state. The row-wise wavelength peaks were taken for each fuel formulation and oxidizer mass flow and then compared.

The results show that the combustion is dominated by wave-like structures and that the most excited frequencies and wavelengths, as well as the flame position and thickness, depend on the fuel

viscosity and oxidizer mass flow. Nevertheless, some limitations have to be taken into account when the results are analyzed. First of all, the analysis is performed on 2D images. This means that what we analyzed can be the superposition of all the combustion phenomena appearing on the fuel surface along the whole width. Moreover, the brightness of the flame and the condensed products which polluted the window increase the complexity of the optical measurement.

5.1.1 Flame height

Fig. 10 shows the dependence of the flame height from the fuel viscosity and oxidizer mass flow.

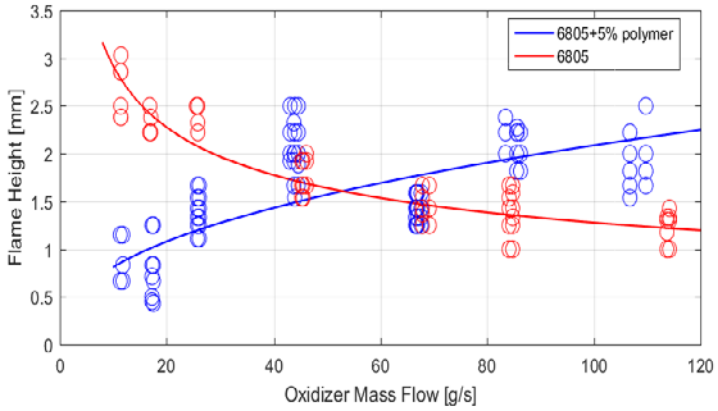

Figure 10: Flame height dependence on fuel composition and oxidizer mass flow

It is possible to notice that the two fuel compositions show a different dependency on the oxidizer mass flow. In particular, the fuel with the lower viscosity (pure paraffin 6805) shows a decreasing flame height with increasing oxidizer mass flow. On the other hand, the flame height of the fuel with the higher viscosity (6805+5%polymer) increases with increasing oxidizer mas flow. The crossing point, where the two compositions have more or less the same flame height, is at around 50 g/s. This trend can be also seen in the frames extracted from the videos.
Figures 11 and 12 show two series of three frames taken from the combustion high-speed videos of respectively pure paraffin 6805 and 6805+5%polymer, at three different oxidizer mass flows (10, 50 and 100 g/s). Here it is possible to see how the flame height of the pure paraffin decreases with increasing oxidizer mass flow, while the flame height of 6805+5%polymer increases.

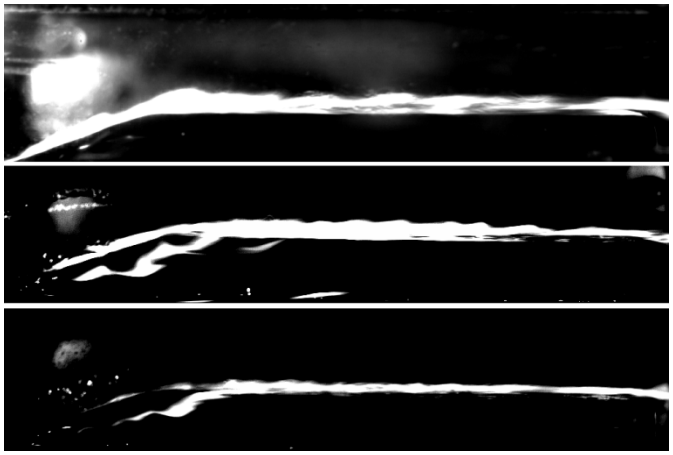

Figure 11: Frames taken from combustion high-speed videos of 6805 at $\dot{m}_{ox} = 10{,}50{,}100\ g/s$ (from top to bottom)

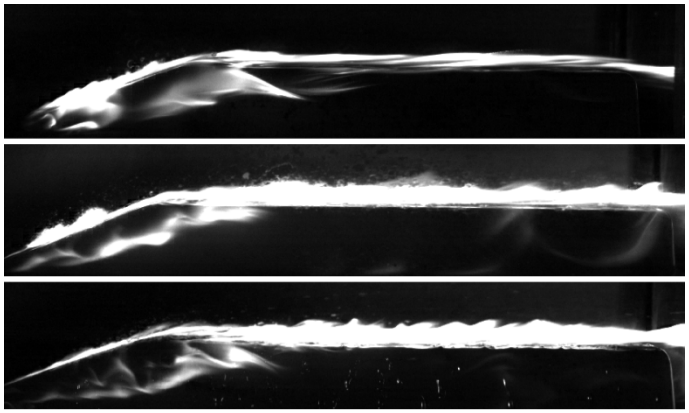

Figure 12: Frames taken from combustion high-speed videos of 6805+5%polymer at $\dot{m}_{ox} = 10{,}50{,}100\ g/s$ (from top to bottom)

This trend can be explained with the extended hybrid theory for liquefying fuels proposed by Karabeyoglu et al. [5], [6]. In fact, according to the liquid layer theory, the regression rate of the so-called liquefying fuels is given from a evaporation regression rate, due to the vaporization of the liquid into the gas stream, and an entrainment regression rate, due to the liquid layer instabilities and droplets entrainment. The sum of these two terms gives the final total regression rate for liquefying fuels. Of course, the single regression rates are influenced from many parameters (fuel properties, combustion conditions, etc.). Both of them strictly depend on the oxidizer mass flux. In particular, for the entrainment regression rate, as already explained in section 4, the roles of fuel viscosity and oxidizer mass flow are very important (a low viscosity and a high oxidizer mass flux are needed in order to reach the instability limit). In fact, at really low mass flows no entrainment takes

place, since no instabilities arise. This is, for example, what happens with the higher viscosity fuel blend (6805+5%polymer) at mass flows lower than 30 g/s (see Fig. 13, 14). On the other hand, the pure paraffin, due to the lower viscosity, is able to reach the minimum critical speed needed to have instabilities, even at low mass flows (see Fig.13, 14).

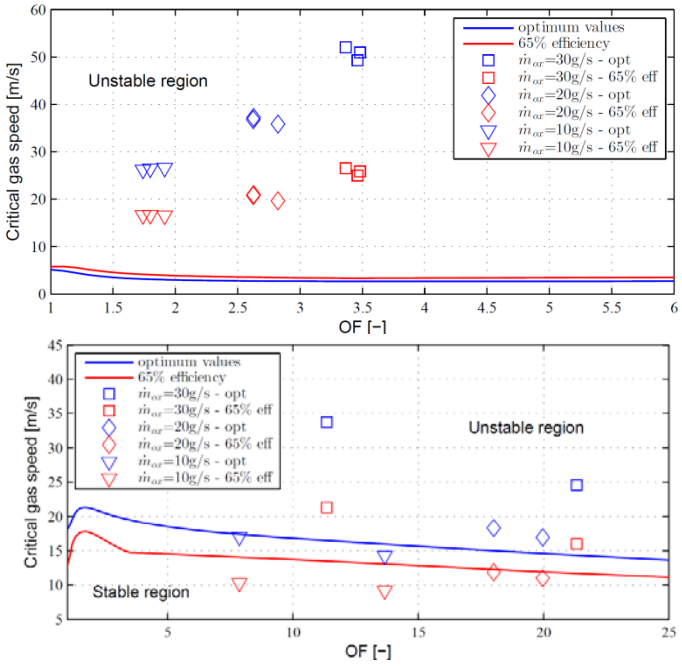

Figure 13: Critical gas speed curves with experimental values for 6805 (top) and 6805+5%polymer (bottom)

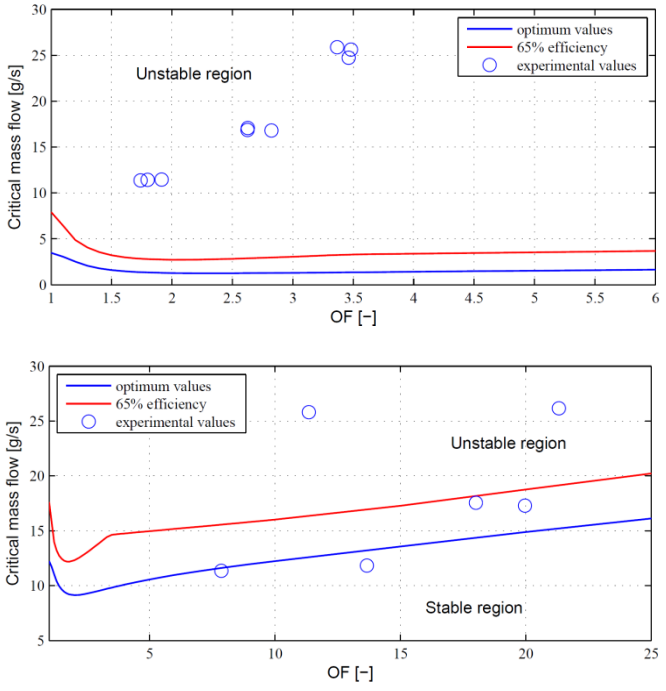

Figure 14: critical mass flows curves with experimental values for 6805 (top) and 6805+5%polymer (bottom)

This means that the balance between these two important parameters (fuel viscosity and oxidizer mass flow) decides whether the vaporization or the entrainment regression rate plays a more important role. In this way it is also possible to explain the trend of the flame height for the two fuels. Pure paraffin 6805 has a lower viscosity and experiences the entrainment phenomenon at every oxidizer mass flows (see Fig. 13,14). According to Karabeyoglu et al. [5] and the Kelvin-Helmholtz instability theory [14], the instabilities and, thus, the droplets entrainment increase as the mass flux increases (in this case the mass flux and flow have the same trend, since the area is almost a constant). Also the vaporization regression rate increases with the oxidizer mass flux, but with a slower slope. In the case of the pure paraffin, it is possible to say that the droplets entrainment dominates direct gasification. When the viscosity is really low, the vaporization from the liquid surface is negligible, meaning that all of the mass is transferred to the gas flow in form of droplets [5]. This brings to an important increase in the regression rate, which can be also see in our burning tests (see Fig. 15), and to a decrease in the liquid layer thickness (see Karabeyoglu et al. [5]). Consequently, also the flame height tends to decrease, since the flame position is strictly connected to the regression rate. For what concerns the fuel with the higher viscosity, no entrainment arises at very low mass flows (10-20 g/s). Therefore, the regression rate is given only from the liquid fuel vaporization and pyrolization. As the oxidizer mass flow increases, the liquid layer becomes unstable, due to the higher shear stresses, and droplets entrainment takes place, thus bringing to a higher regression rate. However, the fuel liquid viscosity is higher than that of the pure paraffin, so the melt layer is less unstable and fewer droplets are able to be entrained in the flow. This means that, in this case, the vaporization regression rate plays still an important role even at high mass flows. Therefore, the evaporation blowing of the gaseous phase mass transfer from the fuel surface is still pretty high. This “pushes” the flame sheet further away from the liquid layer and, consequently, increases the flame height.

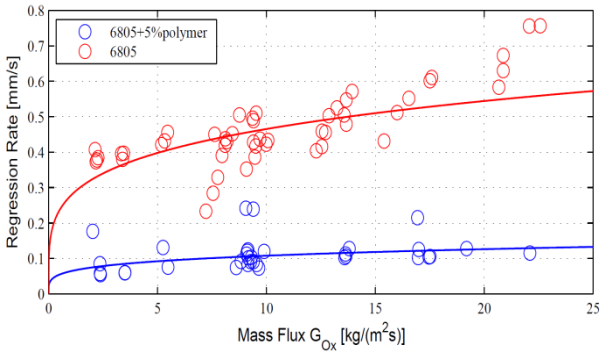

Figure 15: regression rate curves for the analyzed fuel compositions

A more precise way to compute the mean flame height is to automatically detect it from the full frames. In this case, the frames are analyzed in their original size (no cropping is performed) and converted to black and white images. The average fuel grain location is determined by scanning the columns of each frame from the bottom to the top and detecting the edge with the Canny method. The same is done, from the top to the bottom, in order to detect the flame edge. The values of the heights are then saved for each column in each frame and the time average, over 10000 frames, is computed. It is important to stress that the same time span as in the previous analysis was used. The results of this analysis are showed in Fig. 16.

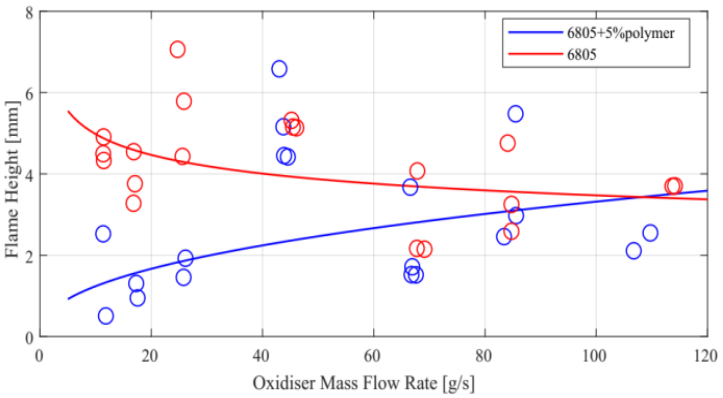

Figure 16: Flame height dependence on fuel composition and oxidizer mass flow (full frames analysis)

The trend is the same like in the previous results: 6805 flame height decreases with increasing oxidizer mass flow, while 6805+5%polymer increases. The same result can be also directly visualized in Fig. 17.

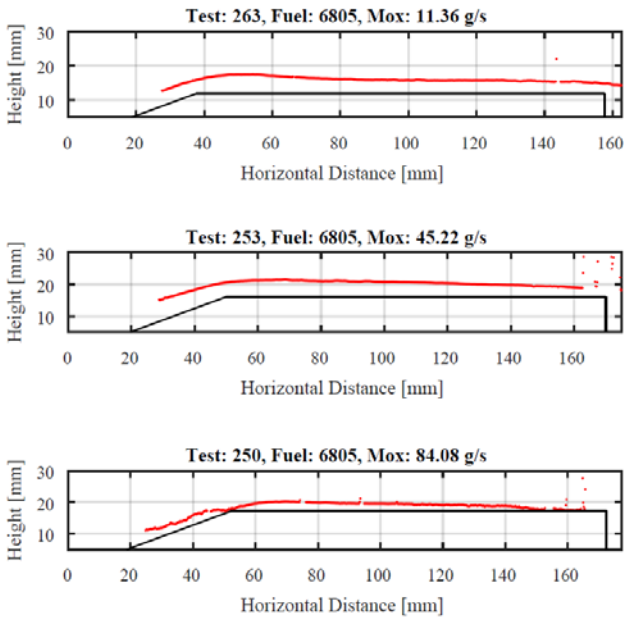

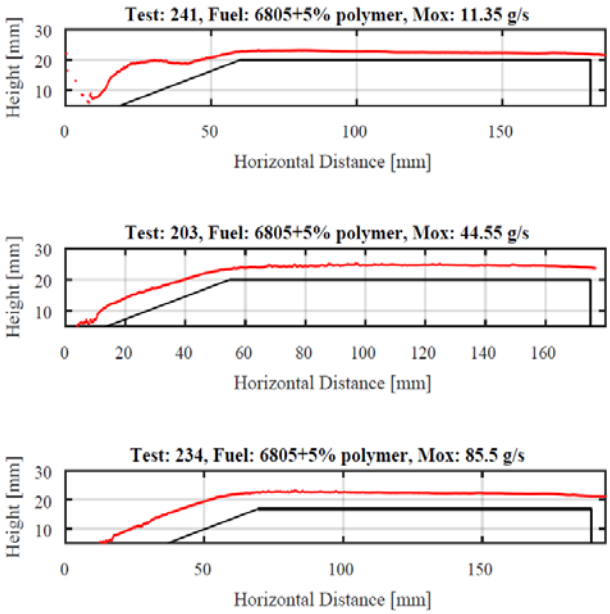

Fig. 17: average flame position (red) and fuel grain position (black) for the two fuel compositions at three oxidizer mass flows

Here, the mean flame height versus horizontal distance is plotted for different combustion tests run with the two fuel compositions and at three different mass flows (about 10, 50 and 100 g/s). The mean fuel grain surface is also plotted. The values of flame height represented in Fig. 15 (one for each test) are both space and time averaged: the space average is computed, for each frame, on the first half of the flat part of the fuel surface; these values are then time averaged over 10000 frames (1 second during steady state, the same like in the previous analysis). It is important to underline that the flame height values in this analysis are higher than those in the previous analysis because in this case the full frames are analyzed. The fuel surface is automatically detected and averaged over time. On the contrary, in the previous analysis, the fuel surface is manually detected by looking only at the first frames during the ignition phase (where the fuel surface is more visible). This means that in this case we probably underestimate the fuel height due to an error in the fuel surface detection.

5.2 CH* chemiluminescence videos

It is generally recognized (see [35], [36], [37]) that the primary species contributing to flame luminescence are the electronically excited species CH*, C_2* and OH*. All three species show a close correspondence across the main reaction zone and are thus equally suitable as markers for the flame zone location. In particular, the concentrations of CH* increase rapidly to a maximum within the flame and then decay rapidly

downstream of the reaction zone [37]. Therefore, CH* chemiluminescence videos were recorded and analyzed, as explained in Sec. 3. Like for the high-speed videos, the analysis was carried out on 1 second during steady-state. The contour plots of the spatial coefficients coming from both decomposition algorithms were plotted for all the CH* videos. Interesting information on the flame topology can be drawn from the contour plot of the spatial coefficients of the first POD mode. It shows the typical profile of combustion over a flat fuel surface with a turbulent boundary layer. The structure of the main diffusion flame above the fuel grain can be easily recognized. The contour plots of higher POD modes show combustion fluctuations, as it can be noticed from the increased intensity and variations of the flame. For what concerns the contour plots of the independent components, no flame profile can be seen. Instead, independent burning regions over the fuel surface are highlighted in each component.

5.2.1 Flame topology and location

In Fig. 18 and 19 the contour plots of the first POD mode of, respectively, 6805 and 6805+5%polymer at three different oxidizer mass flows are shown. It can be clearly seen that, for both fuel compositions, the flame surface becomes more unstable and rough as the oxidizer mass flow increases. More “droplets” detaching from the main flame can be noticed. Moreover, by comparing the two fuel compositions at the same oxidizer mass flow, it is distinctly visible that the pure paraffin presents a more unstable flame surface, with more droplets. The CH* flame intensity is also higher for 6805, due to the higher temperatures (note also that, at the same oxidizer mass flow, more fuel burns with the pure paraffin with respect to the paraffin blend, due to the higher regression rate. This means that the mixture ratio OF is smaller for 6805 than for 6805+5%polymer. This brings to higher temperature in the combustion chamber).

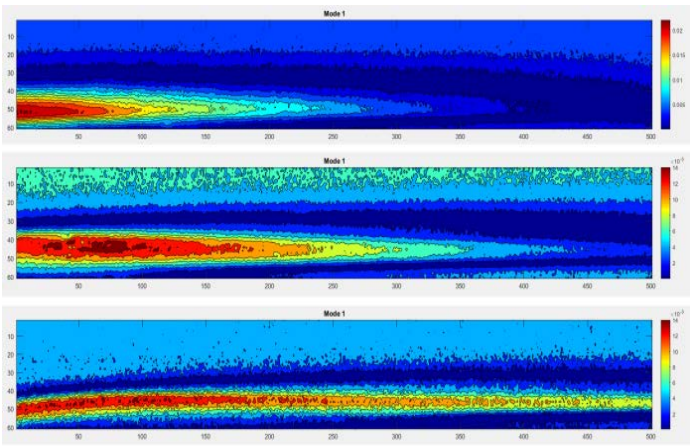

Figure 18: Contour plots of the first POD mode of 6805 at $\dot{m}_{ox} = 10, 50, 100\ g/s$ (from top to bottom). The two axes are in pixels.

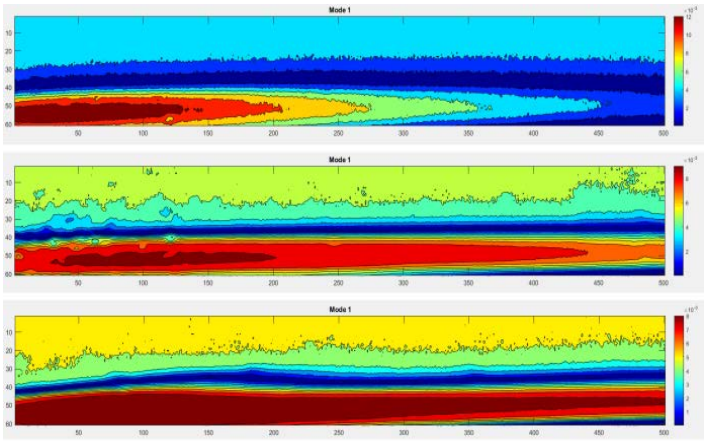

Figure 19: Contour plots of the first POD mode of 6805+5%polymer at $\dot{m}_{ox} = 10, 50, 100\ g/s$ (from top to bottom). The two axes are in pixels.

By looking at the contour plots, some similarities in the flame topology can be recognized. In fact, in all of them, there is a region on the bottom with a high CH* intensity, followed by an area where the CH* emission goes almost to zero and then a region on the surface where the CH* intensity increases again. The region on the bottom, with the maximum CH* intensity emission, corresponds to the fuel rich zone near the fuel surface. Here the fuel gases vaporized from the melt layer and the fuel droplets can already react with the oxidizer gases, thus producing CH* species (the dominant source of CH* chemiluminescence, according to Devriendt et al. [36], is the reaction $\mathrm{C_2H + O = CO + CH^*}$). The region where almost no CH* are emitted corresponds to the main flame sheet. Here OH* are more likely to be produced (according to Gaydon [35], OH* is primarily formed by the reaction $CH + O_2 = CO + OH^*$). The droplets that are not burnt under the main flame are transported over the flame sheet by the combustion products flow and here, in the oxidizer-rich region of the boundary layer, finally burnt. This area corresponds to the region on the surface, over the main flame, where the CH* emission increases again. Moreover, it is possible to notice that the region with the maximum CH* emission becomes more concentrated in the tests with pure paraffin. This is due to the higher regression rate characterizing the fuel with lower viscosity. As already explained in the previous section, the entrainment regression rate dominates, in this case, over the vaporization regression rate, thus reducing the effective heat of gasification and the blocking factor in the boundary layer. On the other hand, the vaporization regression rate plays still an

important role in the combustion of the 6805+5%polymer. This brings to a lower regression rate and a wider reaction zone. It can be also seen that the flame height has more or less the same trend like in the high-speed video results. At the lower mass flow (about 10 g/s), 6805 shows a higher flame than the other fuel composition. At about 50 g/s, both fuels have more or less the same flame height. At the higher mass flow (about 100 g/s), the higher viscosity fuel is characterized by a higher flame. Finally, it can be recognized that, at every oxidizer mass flow, the main flame zone (the region where the CH* emission is almost zero) for the higher regression rate fuel is thicker than the flame zone of the slower burning fuel. However, for a better analysis of the main flame sheet, OH* chemiluminescence images of the burning tests would be needed.

6. CONCLUSIONS

The combustion behaviour of different paraffin-based 2D fuel slab samples burning with GOX was investigated with an optical combustion chamber. High speed video and CH* chemiluminescence imaging enables the collection of a huge amount of data, which needs to be analysed in detail. Therefore, two automated data evaluation techniques, based on POD and ICA, were applied to the analysis of the luminosity field of images in a reactive flow. This allows for an analysis of the considered scalar field by identifying leading components during the burning process. POD and ICA were applied separately to the same luminosity data. The results obtained prove the robustness of the two decomposition methods and the effectiveness of the video analysis process. In particular, in this work, the flame characteristics with different fuels and oxidizer mass flows were studied. It was shown that the flame location and topology depend on the fuel viscosity and oxidizer mass flow. This work is part of a wider study on the liquid layer instability process (Kelvin-Helmholtz instability), which is important to better understand the onset and development of the entrainment process.

Two main test campaigns were performed with two different fuel compositions: pure paraffin 6805 and the same paraffin with 5% polymer. Fuel slabs with 20° forward facing ramp were used, due to the better flame holding and continuous flame front. In both test campaigns, the oxidizer mass flow was varied in a range from 10 to 120 g/s. From the results it is shown that the flame location depends on the fuel composition and oxidizer mass flow choice. In particular, the trend was shown to be different for the two investigated fuels. For the higher viscosity fuel, the flame height is increasing with increasing oxidizer mass flow. On the other hand, for the lower viscosity fuel, the flame becomes thinner as the oxidizer mass flow increases. This is due to the more or less important role of the vaporization regression rate with respect to the entrainment one. The importance of these two players is influenced by the fuel viscosity (at constant oxidizer mass flow). Moreover, from the CH* video imaging, it was noticed that the region with the higher CH* emission is thinner and more concentrated in the tests with pure paraffin. This is also due to the higher regression rate of 6805 with respect to the paraffin-polymer blended fuel. Finally, it is also possible to recognize that the main flame zone becomes thicker for the higher regression rate fuel composition. However, for a deeper analysis of the flame sheet, further investigations with OH* video imaging are required.

ACKNOWLEDGMENTS

This work was partially funded by the DLR project ATEK (Antriebstechnologien und Komponenten für Trägersysteme: Propulsion Technologies and Components for Launcher Systems). The support of the M11 team and the propellants department is greatly acknowledged.

NOMENCLATURE

B	Constant for the perturbation expression
G_{Ox}	Oxidizer mass flux
$K_{0,1,2}$	Dispersion relation constants
U	Gas velocity
a,n	Regression rate parameters
g	Gravity acceleration
h	Height
k	Wave number
$\dot{m}_{Ox}$	Oxidizer mass flow
r_f	Regression rate
t	Time
x	Longitudinal coordinate
γ	Surface Tension
μ	Kinetic viscosity
ρ	Density
ω	Wave frequency

SUBSCRIPTS

G	Gas
I	Imaginary part
L	Liquid
R	Real part

Acronyms/Abbreviations

DLR	German Aerospace Center
GOX	Gaseous Oxygen
HRE	Hybrid Rocket Engines
HDPE	High-Density Polyethylene
HTPB	Hydroxyl-Terminated Polybutadiene
KHI	Kelvin-Helmholtz instability
ICA	Independent Component Analysis
POD	Proper Orthogonal Decomposition

REFERENCES

[1] A. Karabeyoglu, J. Stevens, D. Geyzel, B. Cantwell and D. Micheletti, "High Performance Hybrid Upper Stage Motor," in *47th AIAA/ASME/SAE/ASEE Joint Propulsion Conference and Exhibit*, 2011.

[2] G. Marxman and M. Gilbert, "Turbulent Boundary Layer Combustion in the Hybrid Rocket," in *9th Symposium (International) on Combustion*, Elsevier, 1963, pp. 371-383.

[3] M. Chiaverini, "Review of Solid-Fuel Regression Rate Behavior in Classical and Nonclassical Hybrid Rocket Motors," in *Fundamentals of Hybrid Rocket Combustion and Propulsion*, American Institute of Aeronautics and Astronautics, 2007, pp. 37-126.

[4] A. Karabeyoglu, B. J. Cantwell and D. Altman, "Development and Testing of Paraffin-based Hybrid Rocket Fuels," in *37th AIAA/ASME/SAE/ASEE Joint Propulsion Conference and Exhibit*, Salt Lake City, Utah, 2001.

[5] A. Karabeyoglu, D. Altman and B. J. Cantwell, "Combustion of Liquefying Hybrid Propellants: Part 1, General Theory," *Journal of Propulsion and Power*, Vol.18, pp. 610-620, 2002.

[6] A. Karabeyoglu and B. J. Cantwell, "Combustion of Liquefying Hybrid Propellants: Part 2, Stability of Liquid Films," *Journal of Propulsion and Power*, Vol. 18, pp. 621-630, 2002.

[7] A. Petrarolo, M. Kobald and S. Schlechtriem, "Optical Analysis of the Liquid Layer Combustion of Paraffin-based Hybrid Rocket Fuels," in *EUCASS*, Milano, 2017.

[8] A. Petrarolo, M. Kobald and S. Schlechtriem, "Liquid Layer Combustion Visualization of Paraffin-Based Hybrid Rocket Fuels," in *53th AIAA/ASME/SAE/ASEE Joint Propulsion Conference*, 2017.

[9] A. Petrarolo, M. Kobald, H. K. Ciezki and S. Schlechtriem, "Optical Analysis of Liquid Film Instabilities in Paraffin-Based Hybrid Rocket Fuels," in *68th International Astronautical Congress (IAC)*, 2017.

[10] M. Kobald, C. Schmierer, H. K. Ciezki, S. Schlechtriem, E. Toson and L. T. D. Luca, "Viscosity and Regression Rate of Liquefying Hybrid Rocket Fuels," *Journal of Propulsion and Power*, pp. 1-7, 2017.

[11] A. D. D. Craik, "Wind Generated Waves in Thin Liquid Films," *Journal of Fluid Mechanics*, Vol. 26, Pt.2, pp. 369-392, 1966.

[12] I.-D. Chang and P. E. Russel, "Stability of a Liquid Layer Adjacent to a High-Speed Gas Stream," *Physics of Fluids*, Vol. 8, No. 6, pp. 1018-1026, 1965.

[13] R. S. Amano, Y.-H. Yen, T. C. Miller, A. Ebnit, M. Lightfoot and V. Sankaran, "Study of the Liquid Breakup Process in Solid Rocket Motor," *Journal of Spacecraft and Rockets*, vol. 53, pp. 980-992, 2016.

[14] T. Funada and D. D. Joseph, "Viscous potential flow analysis of Kelvin-Helmholtz instability in a channel," *Journal of Fluid Mechanics*, vol. 445, 2001.

[15] M. Ishii and M. A. Grolmes, "Inception criteria for droplet entrainment in two-phase concurrent film flow," *AIChE Journal*, vol. 21, pp. 308-318, 1975.

[16] R. A. Gater and M. R. LÉcuyer, "A Fundamental Investigation of the Phenomena that Characterize Liquid Film Cooling," *International Journal of Heat and Mass Transfer*, Vol. 13, No. 3, pp. 1925-1939, 1970.

[17] I. Nakagawa and S. Hikone, "Study on the Regression Rate of Paraffin-Based Hybrid Rocket Fuels," *Journal of Propulsion and Power*, Vol.27, pp. 1276-1279, 2011.

[18] A. A. Chandler, E. T. Jens, B. J. Cantwell and G. S. Hubbard, "Visualization of the liquid layer combustion of paraffin fuel at elevated pressures," in *63rd International Astronautical Congress*, 2012.

[19] E. T. Jens, P. Narsai, B. Cantwell and G. S. Hubbard, "Schlieren Imaging of the Combustion of Classical and High Regression Rate Hybrid Rocket Fuels," in *50th AIAA/ASME/SAE/ASEE Joint Propulsion Conference*, 2014.

[20] E. T. Jens, A. A. Chandler, B. Cantwell, G. S. Hubbard and F. Mechentel, "Combustion Visualization of Paraffin-Based Hybrid Rocket Fuel at Elevated Pressures," in *50th AIAA/ASME/SAE/ASEE Joint Propulsion Conference*, 2014.

[21] Y. Wada, Y. Kawabata, T. Itagaki, K. Seki, R. Kato, N. Kato and K. Hori, "Observation of combustion behavior of low melting temperature fuel for hybrid rocket using double slab motor," in *10th International Symposium on Special Topics in Chemical Propulsion*, 2014.

[22] M. Kobald and S. Schlechtriem, "Investigation of different Hybrid Rocket Fuels in a 2D Slab Burner with Optical Techniques," in *Tenth International Conference on Flow Dynamics*, 2013.

[23] M. Kobald, H. K. Ciezki and S. Schlechtriem, "Optical Investigation of the Combustion Process in Paraffin-based Hybrid Rocket Fuels," in *49th AIAA/ASME/SAE/ASEE Joint Propulsion Conference*, 2013.

[24] M. Kobald, I. Verri and S. Schlechtriem, "Theoretical and experimental analysis of liquid layer instability in hybrid rocket engines," *CEAS Space Journal*, vol. 7, pp. 11-22, 2015.

[25] A. Petrarolo and M. Kobald, "Evaluation techniques for optical analysis of hybrid rocket propulsion," *Journal of Fluid Science and Technology*, vol. 1 , 2016.

[26] A. Petrarolo, M. Kobald and S. Schlechtriem, “Understanding Kelvin–Helmholtz instability in paraffin-based hybrid rocket fuels,” *Experiments in Fluids*, p. 59:62, 2018.

[27] M. Kobald, E. Toson, H. Ciezki, S. Schlechtriem, S. di Betta, M. Coppola and L. T. DeLuca, “Rheological, optical, and ballistic investigations of paraffin-based fuels for hybrid rocket propulsion using a two-dimensional slab-burner,” *EUCASS Proceedings Series - Advances in AeroSpace Sciences*, Vol. 8, pp. 263-282, 2016.

[28] H. K. Ciezki, J. Sender, W. Clau-oslash, A. Feinauer and A. Thumann, “Combustion of Solid-Fuel Slabs Containing Boron Particles in Step Combustor,” *Journal of Propulsion and Power*, vol. 19, pp. 1180-1191, 2003.

[29] M. Kobald and E. Toson, “Evaluation of Paraffin-based Fuels for Hybrid Rocket Engines,” in *50th AIAA/ASME/SAE/ASEE Joint Propulsion Conference*, 2014.

[30] G. Kerschen, J.-c. Golinval, A. F. Vakakis and L. A. Bergman, “The Method of Proper Orthogonal Decomposition for Dynamical Characterization and Order Reduction of Mechanical Systems: An Overview,” *Nonlinear Dynamics*, vol. 41, pp. 147-169, 2005.

[31] K. Bizon, S. Lombardi, G. Continillo, E. Mancaruso and B. M. Vaglieco, “Analysis of Diesel engine combustion using imaging and independent component analysis,” *Proceedings of the Combustion Institute*, vol. 34, pp. 2921-2931, 2013.

[32] K. Bizon, G. Continillo, E. Mancaruso, S. S. Merola and B. M. Vaglieco, “POD-based analysis of combustion images in optically accessible engines,” *Combustion and Flame*, vol. 157, pp. 632-640, 2010.

[33] K. Kuo and R. Houim, “Theoretical Modeling and Numerical Simulation Challenges of Combustion Processes of Hybrid Rockets,” in *47th AIAA/ASME/SAE/ASEE Joint Propulsion Conference and Exhibit*, 2011.

[34] N. Pelletier, “Etude des Phenomenes de Combustion dans un Propulseur Hybride. Modelisation et Analyse Experimentale de la Regression des Combustibles Liquefiables,” 2009.

[35] A. G. Gaydon, Spectroscopy of Flames, Chapman and L. Hall, Eds., 1957.

[36] K. Devriendt, H. Van Hook, B. Ceursters and J. Petters, *Chem. Phys. Lett.*, vol. 261, pp. 450-456, 1996.

[37] R. W. Schefer, “Flame Sheet Imaging Using CH Chemiluminescence,” *Combustion Science and Technology*, Vols. 126: 1-6, pp. 255-279, 2010.